Nanomed J. 12(2): 279-288, Spring 2025

RESEARCH PAPER

Paper strip sensor based on γ-fe_2O_3@prussian blue nanozyme for H_2O_2 detection

Zoha Babaei Afrapoli [1], Sharmin Kharrazi [1], Fardin Amidi [2], Ramin Rahimnia [1], Reza Faridi-Majidi [1]*

[1]Department of Medical Nanotechnology, School of Advanced Technologies in Medicine, Tehran University of Medical Sciences (TUMS), Tehran, Iran
[2]Department of Anatomy, School of Medicine, Tehran University of Medical Sciences (TUMS), Tehran, Iran

ABSTRACT

Objective(s): High levels of hydrogen peroxide (H_2O_2) induce oxidative stress in physiological environments. Elevation of H_2O_2 levels in semen can be a reason for male infertility, by causing protein and enzyme denaturation, lipid peroxidation, and DNA damage. Oxidative stress can affect sperm features, such as viability, motility, and fertilization potential. Although nanozymes are widely used to detect H_2O_2 using different techniques, monitoring of H_2O_2 in physiological fluids remains a challenge that has not been studied extensively. We report on a non-enzymatic paper strip based on γ-Fe_2O_3@Prussian blue nanoparticles (γ-Fe2O3@PB NPs) and their performance for H_2O_2 detection in buffer and seminal plasma.

Materials and Methods: γ-Fe_2O_3 NPs were synthesized using chemical coprecipitation method and were then coated with PB. γ-Fe_2O_3@PB NPs were characterized using ultraviolet-visible spectroscopy (UV-vis), dynamic light scattering (DLS), X-ray diffraction (XRD), and transmission electron microscopy (TEM). The results confirmed formation of relatively monodisperse and approximately 71 nm γ-Fe_2O_3@PB NPs. The peroxidase-like activities of γ-Fe_2O_3 NPs and γ-Fe_2O_3@PB NPs were measured using UV-visible spectroscopy.

Results: The results demonstrated that the catalytic activity of γ-Fe_2O_3@PB NPs was higher than that of γ-Fe¬$_2$¬O_3 NPs. The concentrations of γ-Fe_2O_3@PB NPs and TMB, immobilized on paper strips, were optimized. The detection limit of the constructed lateral flow assays (LFA) for H_2O_2 in acetate buffer was 50.0 µM. Citric acid and ascorbic acid, as common components in semen, showed interference with the performance of paper strips. The γ-Fe_2O_3@PB NPs-based paper strip could detect H_2O_2 spiked in human seminal plasma in 20 min with a detection limit of 750.0 µM.

Conclusion: The colorimetric detection of H_2O_2 on paper strips was successful and quantification of the results was possible with the help of a cell phone, which makes it a breakthrough in quantitative rapid tests.

Keywords: *Fe_2O_3 nanoparticles, Hydrogen peroxide, Male infertility, Nanozymes, Paper strip*

How to cite this article
Babaei Afrapoli Z, Kharrazi Sh, Amidi F, Rahimnia R, Faridi-Majidi R. Paper Strip Sensor Based on γ-Fe_2O_3@Prussian Blue Nanozyme for H_2O_2 Detection. Nanomed J. 2025; 12(1): 279-288. DOI: 10.22038/nmj.2024.79710.1968

INTRODUCTION

Detection of hydrogen peroxide (H_2O_2) is essential in many fields, such as food security, pharmaceutical, clinical, and environmental protection [1]. H_2O_2 is the most stable member of the reactive oxygen species (ROS) family [1-3]. Although H_2O_2 is vital for normal cell function, its high levels cause oxidative stress in physiological environments [4]. According to the report by Ransy et al., H_2O_2 in the concentration range of 100-500 µM can generate oxidative damage in cell models [5]. H_2O_2 is also a by-product of oxidase enzymes, such as glucose oxidase, cholesterol oxidase, and alcohol oxidase [6, 7].

Many studies have introduced various H_2O_2 detection methods, including chromatography [8], electrochemical [9, 10], enzymatic, luminescent [6], and fluorescence [9, 11] techniques. Although these methods are highly precise for H_2O_2 detection, they suffer from some drawbacks, such as need for expensive equipment, expert users, rigorous storage conditions of the reaction solution for a long time, and not being portable [12]. Paper-based analytical devices (PADs) are

* *Corresponding author: Email: refaridi@sina.tums.ac.ir*
Note. This manuscript was submitted on May 4, 2024; approved on June 8, 2024

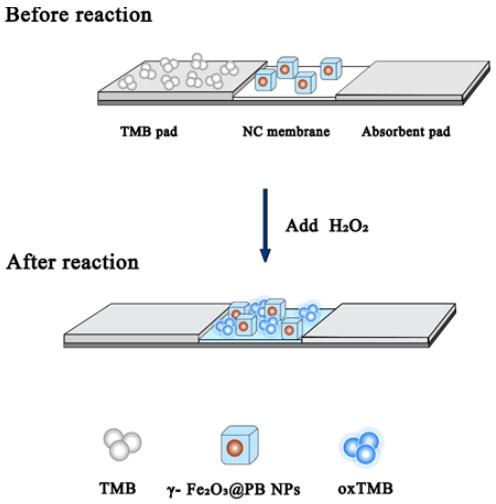

Fig. 1. Illustration of the structure and performance of paper strip sensor based on γ-Fe2O3@prussian blue NPs for the detection of H_2O_2

promising for point-of-care testing (POCT), owing to their ease of use, low cost, and portability [13]. Paper-based microfluidics (μPADs) and lateral flow assays (LFAs) are two common PADs that have been widely studied [14]. The fabrication of μPADs usually requires expensive lithography, wax printing, or cutting devices, and the possibility of large-scale fabrication of these types of tests remains a challenge [15, 16]. The LFA method is based on interacting biomolecules with analytes in the test and control lines [17]. The only study performed for detection of H_2O_2 using the lateral flow assay is reported by Fung et al. [18]. They used horseradish peroxidase (HRP) as a recognition element for H_2O_2 detection. They immobilized HRP on the detection zone of the LFA substrate using four patterns: a) biotinylated HRP interacting with avidin in the detection zone, b) HRP interacting with anti-HRP antibodies in the detection zone, c) goat anti-mouse immunoglobulin G (IgG)-HRP immobilized on the detection zone, and d) physical adsorption. Although HRP immobilized on the detection zone by biotin-avidin and antigen-antibody interactions has appropriate sensitivity for H_2O_2 detection, immobilization process of HRP s is expensive and requires complex conjugation procedures. Hence, there is a demand for a cost-effective paper-based diagnostic approach that employs accurate recognition elements as enzyme substitutes, without relying on expensive manufacturing equipment.

In the past decades, various nanomaterials, such as noble metals, metal oxides, metal sulfides/ metal selenides, carbon materials, and metal-organic frameworks (MOFs), have been widely used as artificial enzymes [19, 20]. Nanozymes are a class of artificial enzymes with intrinsic enzyme-like activity [21, 22]. Compared to natural enzymes, nanozymes have advantages such as low cost, high stability, easy modification, and easy storage [19, 23-25]. Hence, they have been widely used for H_2O_2 detection [6, 8, 9].

In the present study, we used γ-Fe_2O_3@ Prussian blue nanoparticles (γ-Fe_2O_3@PB NPs) with peroxidase-like activity instead of HRP for the detection of H_2O_2. A non-enzymatic paper strip based on γ-Fe_2O_3@PB NPs was fabricated, and its performance was assessed for H_2O_2 detection. Human semen samples were selected as a model of physiological fluid because Oxidative stress can affect sperm parameters such as viability, motility, and fertilization potential by causing structural and performance deficiencies at the biomolecular level. [2, 4, 26]. In addition, high levels of ROS have been reported in 30 – 80 % of infertile men [27]. To the best of our knowledge, there are no reports on the construction of colorimetric paper strip sensors using γ-Fe_2O_3@ PB NPs to detect H_2O_2 in human semen. Earlier, in 2020 and 2021, Blanco et al. and Promsuwan et al. developed electrochemical sensors based on the peroxidase-like activity of nanoparticles to detect H_2O_2 in human semen [4, 28]. However, the electrochemical method needs precise electronic measurement system and analysis instruments in addition to trained experts. The electrochemical method is also more expensive than PADs, and its repeatability is low, which are not applicable to electrochemical sensors, and the results can be observed with naked eye.

MATERIALS AND METHODS

Materials

Ferric chloride ($FeCl_3.6H_2O$), sodium sulfite (Na_2SO_3), ammonium hydroxide solution (NH3. H_2O), dimethyl sulfoxide (DMSO), 3,3',5,5'-tetramethylbenzidine (TMB), potassium ferrocyanide (K4(Fe-(CN)6).3H_2O), anhydrous sodium acetate, acetic acid, ascorbic acid, citric acid, and acetone purchased from Merck (Germany). The conjugate pad (PT1-05), nitrocellulose membrane (NCM) (LFNC-c-ss03- 15 μ), and absorbent pad (SP 08) were purchased from Nupore Filtration Systems Pvt. Ltd. (India).

Preparation of γ-Fe_2O_3@PB NPs

γ-Fe_2O_3 NPs were synthesized using a coprecipitation method developed by Sun et al. [29] with some modifications. Briefly, 3 mL of $FeCl_3.6H_2O$ (2 M) was prepared in 2 M HCl and then added to 10.33 mL of deionized (DI) water. Subsequently, 2 mL of Na_2SO_3 (1 M) was added dropwise to the solution. The solution color changed from bright yellow to red. The yellow solution was rapidly added to NH3.H_2O solution (0.85 M) with vigorous stirring. A black precipitate was immediately obtained, and the solution was stirred for 30 min. The black precipitate was washed with deoxygenated water by magnetic decantation until the pH dropped below 7.5. Half of the precipitate was diluted with 84 mL of DI water, and the pH was adjusted to 3. The temperature of the solution was raised to 90 °C within 5 min. The solution was then stirred at 100 °C for 60 min under aeration. The resulting red-brown γ-Fe_2O_3 NPs were washed four times with DI water via magnetic decantation. Subsequently, γ-Fe_2O_3 NPs were coated with PB using a single precursor method. First, the concentration of γ-Fe_2O_3 NPs was set at 0.1 mg mL^{-1}, and the pH was adjusted to 2 with HCl (0.1 M). An appropriate amount of K4(Fe-$(CN)_6$).3H_2O (10 mg mL^{-1}) was then added dropwise to γ-Fe_2O_3 NPs under gentle stirring. The final concentration of K_4(Fe-$(CN)_6$).3H_2O in the solution was adjusted to 2.5 mg mL^{-1}. The solution was mixed for 1 hr and centrifuged until the supernatant became colorless [30].

Characterization

The size and morphology of PB-Fe_2O_3 NPs were examined by means of transmission electron microscopy (TEM) (ZEISS, EM10C-100 KV, Germany). The ultraviolet-visible (UV-vis) absorption spectrum was recorded using a Cytation 3 plate reader (BioTek, USA). The hydrodynamic size and zeta potential of the nanoparticles were measured using a ScatterOScope (I) (SOSI, K-ONE, South Korea) particle size analyzer and Malvern Zetasizer Nano-ZS ZEN 3600, respectively. The Fe ion concentration in γ-Fe_2O_3 NPs solution was determined using inductively coupled plasma optical emission spectroscopy (ICP-OES) (Vista-PRO, Varian). X-ray diffraction (XRD) pattern was recorded using a PHILIPS PW1730 (λ=0.154056 nm) at a current of 30 mA and a voltage of 40 KV.

Peroxidase-like activity measurement

To evaluate the peroxidase-like activity of γ-Fe_2O_3 and γ-Fe_2O_3@PB NPs, the catalytic oxidation of TMB by γ-Fe_2O_3 and γ-Fe_2O_3@PB NPs was investigated in the presence of H_2O_2. Reaction solutions, including acetate buffer (0.1 M, pH=4) and TMB (0.8 Mm) was treated with: (A) 1.0 Fe µg/mL γ-Fe_2O_3 NPs or γ-Fe_2O_3@PB NPs, (B) 250.0 mM H_2O_2, and (C) 1.0 Fe µg/mL γ-Fe_2O_3 NPs or γ-Fe_2O_3@PB NPs with 250.0 mM of H_2O_2. The absorbance of the reaction solution at 652 nm was measured using a UV-vis spectrophotometer. Steady-state kinetic analysis of γ-Fe_2O_3@PB NPs was performed in the presence of TMB and H_2O_2. Kinetic analysis of γ-Fe_2O_3@PB NPs with TMB as the substrate was performed by adding a constant amount of H_2O_2 (final concentration of 250.0 mM) to the various concentrations (0, 0.075, 0.150, 0.300, 0.500, 0.650, and 0.800 mM) of TMB solution. The kinetic analysis of γ-Fe_2O_3@PB NPs with H_2O_2 as the substrate was carried out by adding a constant amount of TMB (0.800 mM) to the various concentrations of H_2O_2 (0, 31.0, 62.0, 125.0, 250.0, and 500.0 mM). The absorption data were then fitted to the Michaelis–Menten equation (1) to calculate the kinetic parameters.

$$V_0 = V_{max}([S]/[S])+K_m) \quad (1)$$

The Michaelis-Menten equation explains the relationship between the rates of substrate conversion by an enzyme and substrate concentration. In this equation, V_0 is the rate of conversion, Vmax is the maximum rate of conversion, [S] is the substrate concentration, and KM is the Michaelis-Menten constant, which is equivalent to the substrate concentration at which the rate of conversion is half of Vmax and describes the affinity of the enzyme for the substrate.

Real sample collection

In this study human semen specimens were selected as a real sample. For the collection of human semen specimens, ethics approval was obtained from the ethics committee of Tehran University of Medical Sciences, Tehran, Iran (IR.TUMS.MEDICINE.REC.1401.526) and individual volunteers signed the consent to participate in the study. A human semen specimen was obtained from a healthy volunteer and was immediately frozen.

UV-visible spectrophotometric detection of H_2O_2 in buffer and real sample

For the detection of H_2O_2 with UV-vis absorption

spectroscopy, various concentrations of H_2O_2 (0.5-1000 µM), diluted γ-Fe_2O_3@PB NPs with the ratio of 1:25, and 0.800 mM of TMB were prepared in 250 µL acetate buffer (0.1 M, pH=4). After 20 min incubation, the absorbance of each reaction solution was measured at 650 nm wavelength. To measure H_2O_2 in real samples, human semen samples were liquified by incubation for 37 °C over 20 min. The semen sample was centrifuged at 2500 rpm for 6 min to obtain seminal plasma from the whole semen. Subsequently, aliquots of seminal plasma, H_2O_2 with a concentration range of 0.5-1000 µM, γ-Fe_2O_3@PB NPs with dilution ratio of 1:25, and TMB with the concentration of 0.800 mM were prepared in 250 µL acetate buffer. After 20 min, the absorbance of the reaction solutions was recorded at a wavelength of 650 nm.

Assembling paper strip

The designed paper strip consists of three parts: the TMB pad, treated with TMB, NCM, treated with γ-Fe_2O_3@PB NPs, and untreated absorbent pad. All these parts were placed on a backing card. To construct the paper strip, a 12×40 mm^2 NCM was located in the middle of the backing card, a 26×40 mm^2 TMB pad was placed at the bottom of the NCM, and a 22×40 mm^2 absorbent pad was placed at the other end of the NCM. Then, they were cut into 4 mm wide and 56 mm long strips.

Optimising γ-Fe_2O_3@PB NPs concentration on NCM

To optimize γ-Fe_2O_3@PB NPs concentration on the NCM, four NCMs were immersed in γ-Fe_2O_3@PB NPs with the dilution ratios of 1:100, 1:50, 1:33, and 1:25 for 30 min and were dried. Each of them were incorporated in assembling the paper strips. Then, H_2O_2 (5.0 mM) was injected onto the TMB pad. The concentration ratio of γ-Fe_2O_3@PB NPs that produced the highest RGB ratio was determined to be the optimum concentration ratio of γ-Fe_2O_3@PB NPs. RGB ratio was used for quantitative analysis of the colorimetric response. Intensities of red (R), green (G), and blue (B) colours were determined using Color Detector 2.0, based on Equation (2) [31].

$$\text{RGB ratio}=G/(R+G+B) \quad (2)$$

Optimising TMB Concentration on conjugate pad (TMB pad)

To optimize the TMB concentration, its different concentrations (1.0, 2.0, 3.0, 4.0, and 5.0 mM) were dissolved in acetone and were individually added to the TMB pad with a pipette tip and allowed to dry. Then, they were incorporated into individual paper strips. NextH_2O_2 (1.0 mM) was injected onto the TMB pad to assess the oxidation of TMB and the appearance of a green-blue colour on NCM. The TMB concentration that produced the highest RGB ratio was selected as the optimal concentration.

Analysis of paper strips

Serial dilutions of H_2O_2 in acetate buffer (0.1 M, pH 4) in the concentration range of 0, 1.0, 5.0, 10.0, 50.0, 100.0, 250.0, 500.0, 750.0, 1000.0, and 5000.0 µM were prepared. Then, 70.0 µL of each concentration was dropped onto the TMB pad. The solution moved TMB from the TMB pad to the NCM. On NCM pad, H_2O_2 interacted with the Fe^{2+} ions of the γ-Fe_2O_3@PB NPs. One electron was transferred from Fe^{2+} to H_2O_2, and H_2O_2 was broken down into hydroxyl radicals (●OH). Hydroxyl radicals oxidized TMB, producing a green-blue colour. After 20 min incubation, the reaction was complete, and the appearance of a green-blue colour on the strips was assessed. To perform quantitative analysis of the colorimetric response, the RGB ratio was calculated.

Interference assay

The interference of common substances in semen, such as ascorbic acid, citric acid, and fructose, was investigated separately on detecting H_2O_2 [32]. Hence, citric acid, ascorbic acid, and fructose solutions with the concentrations equivalent to that in semen (25.0 mM, 678.2 µM, and 16.4 mM, respectively) were prepared, [33]. H_2O_2 (1000.0 µM) was added to the prepared citric acid, ascorbic acid, and fructose solutions. Next, the treated samples and control group (1000 µM H_2O_2) were applied to the paper strips. After 20 min, the intensity of the green-blue colour of NCM was recorded and the RGB ratio was evaluated.

Performance of paper strips in real sample

To validate the application of paper strips, the detection of H_2O_2 was evaluated in human semen specimens. The various concentrations of H_2O_2 (0.0-1000.0 µM) were spiked directly into the seminal plasma aliquots. The spiked seminal fluid was then applied to paper strips. Finally, the intensity of the green-blue colour of the paper strips was evaluated after 20 min.

RESULTS AND DISCUSSIONS

Characterization of synthesized NPs

The synthesizedγ -Fe_2O_3 NPs and γ-Fe_2O_3@

PB NPs werecharacterized. As indicated in Fig. 1 a, the XRD pattern of γ-Fe_2O_3 NPs shows (220), (311), (400), (422), (440), and (511) peaks, which are characteristic peaks of cubic spinel structure of γ-Fe_2O_3 [30]. γ-Fe_2O_3 NPs had no obvious absorption peaks, but γ-Fe_2O_3@PB NPs had an absorption peak at 700 nm, as previously reported (Fig. 1 b) [30, 34]. The TEM micrograph shows the cubic morphology of the PB NPs, coating the spherical γ-Fe_2O_3 NPs with an average size of 71.0 ± 9.7 nm (Fig. 1 c and d). The hydrodynamic sizes of γ-Fe_2O_3NPs and γ-Fe_2O_3@PB NPs were 121.0 nm and 384.0 nm, respectively (Fig. 1 e and f), indicating that the hydrodynamic size of NPs increased after coating with PB (Fig. 1 g). However, the increase in the zeta potential of the NPs before and after coating was insignificant (Fig. 1 g). γ-Fe_2O_3 and γ-Fe_2O_3@PB NPs were easily separated by a magnet because of the strong magnetic properties of γ -Fe_2O_3 NPs (Fig. 1 h).

Measurement of peroxidase-like activity

The peroxidase-like activity of γ-Fe_2O_3 and γ-Fe_2O_3@ PB NPs was investigated It was evident that the catalytic activity of γ-Fe_2O_3@ PB NPs was more robust than that of γ-Fe_2O_3 NPs (Fig. 2 a and b). This is because the presence of Fe^{2+} ions on the surface of PB provides more catalytic sites [35]. Mixing of TMB and γ-Fe_2O_3 NPs, TMB and γ-Fe_2O_3@ PB NPs, and TMB and H_2O_2 led to

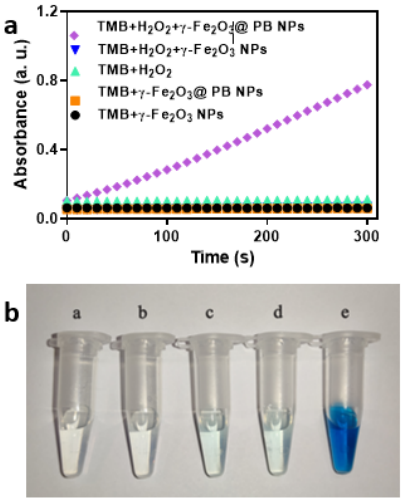

Fig. 2. Time-dependant absorbance changes at 650 nm for the different reaction solutions (a), images of evaluating peroxidase-like activity of the different systems including γ -Fe_2O_3 NPs+TMB (a), γ-Fe2O3@ PB NPs +TMB (b), H_2O_2+TMB (c), γFe_2O_3 NPs+TMB+H_2O_2 (d), and γ-Fe_2O_3@ PB NPs+TMB+H_2O_2 (e)

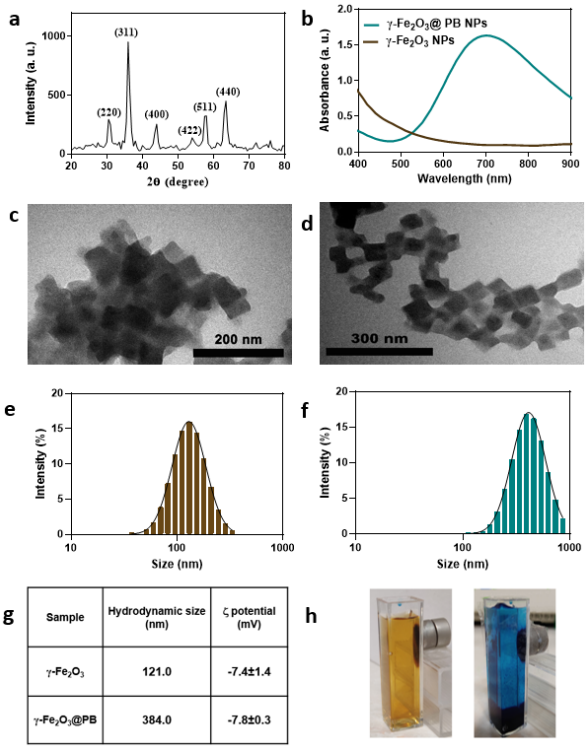

Sample	Hydrodynamic size (nm)	ζ potential (mV)
γ-Fe_2O_3	121.0	-7.4±1.4
γ-Fe_2O_3@PB	384.0	-7.8±0.3

Fig. 1. XRD pattern of γ-Fe_2O_3 NPs (a), UV-visible absorbance spectra of γ-Fe_2O_3 NPs and γ-Fe_2O_3@PB NPs (b), TEM micrograph of γ-Fe_2O_3@ PB NPs (c and d), size distribution of the γ-Fe_2O_3 and γ-Fe_2O_3@ PB NPs by DLS (e and f), table of the hydrodynamic size and zeta potential values of the γ-Fe_2O_3 and γ-Fe_2O_3@ PB NPs (g) photographs of γ-Fe_2O_3 NPs and γ-Fe_2O_3@PB NPs attracted to the magnet (h)

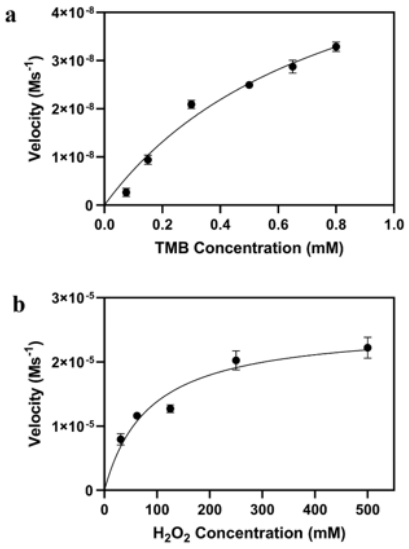

Fig. 3. Steady-state kinetic analysis of γ-Fe_2O_3@ PB NPs. (a) 0.800 mM of TMB as the substrate was added to the various concentrations of H_2O_2, and (b) 250 mM of H_2O_2 as the substrate was added to the various concentrations of TMB

negligible oxidation of TMB, indicating that in the interaction between NPs and H_2O_2, TMB is necessary for the catalytic reaction [36].

Steady-state kinetic parameters were measured for γ-Fe_2O_3@ PB NPs using H_2O_2 and TMB as the substrates. First, the absorption curve was plotted based on the time for each concentration of H_2O_2 and TMB,and the slope was calculated. Then, the velocity of catalytic activity was calculated for each concentration of H_2O_2 and TMB (Fig. 3), and the data were fitted to the Michaelis-Menten equation. The Km values of γ-Fe_2O_3@ PB NPs with TMB and H_2O_2 were obtained 0.694 and 229.6, respectively.

UV-visible spectrophotometric detection of H_2O_2 in buffer and real sample

The UV-vis spectroscopic data demonstrated that the response range for H_2O_2 detection in acetate buffer was 0.5- 250.0 µM and the detection limit was 13.6 µM. H_2O_2 detection in human semen sample was also assessed. The response range for H_2O_2 detection in the semen sample was 1.0-750.0 µM. The detection limit was 91.6 µM. Therefore, the detection limit in the human semen sample was 6.7 times higher than that in the buffer sample. In addition, the upper limit of the response range in the samples that contained seminal plasma was higher than that of the buffer samples. The optical density (OD) of the reaction solution that contained seminal plasma was lower than that of the reaction solution without seminal plasma (Fig. 4). These observations can

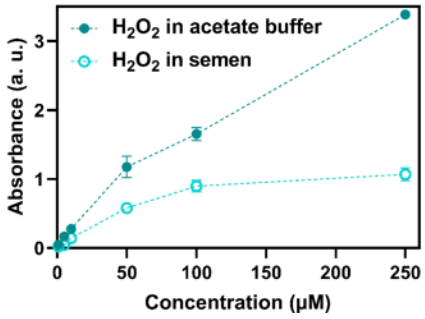

Fig. 4. UV-visible absorption spectrum of H_2O_2 in acetate buffer and human semen samples

be contributed to the presence of antioxidant compounds such as citric acid, ascorbic acid, uric acid, and zinc in the human semen [37].

Optimizing the γ-Fe_2O_3@ PB NPs concentration on NCM

After preparing the paper strip, the concentration of immobilized γ-Fe_2O_3@PB NPs on the NCM was optimized. The colour intensity of the NCM sheet increased by decreasing the dilution ratio of γ-Fe_2O_3@PB NPs from 1:100 to 1:25 (Fig. 5 a). Also, the RGB ratio increased from 0.34 to 0.40 (Fig. 5 b). Thus, a 1:25 concentration ratio of γ-Fe_2O_3@PB NPs was selected as the optimum concentration. The optimal concentration of γ-Fe_2O_3@PB NPs was homogeneously immobilized on the surface of NCM fibers (Fig. 5 c and d).

Optimization of TMB concentration on TMB pad

To determine the optimum concentration of

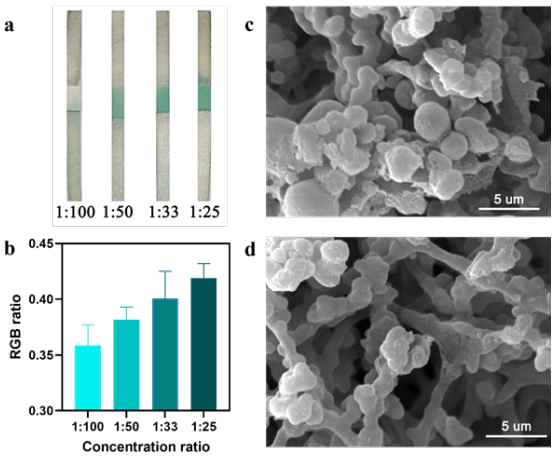

Fig. 5. The optimization of γ-Fe_2O_3@PB NPs concentration on paper strips; the different concentration ratios of γ-Fe_2O_3@PB NPs to the buffer as 1:100, 1:50, 1:33, and 1:25 (a), and their respective RGB ratio bar chart (b), SEM images of NCM before immobilization of γ-Fe_2O_3@PB NPs (c), and after immobilization of γ-Fe_2O_3@PB NPs (d)

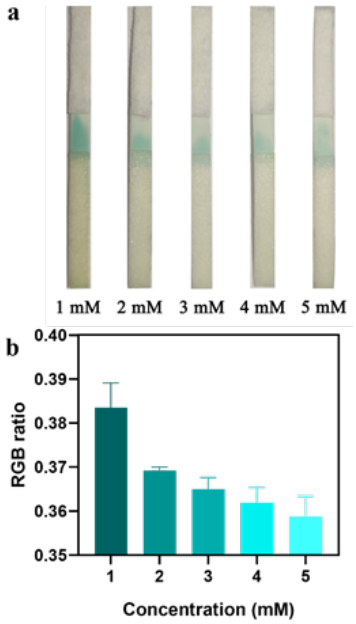

Fig. 6. The photograph of optimizing TMB concentration on paper strips (a) and the respective RGB ratio bar chart (b)

TMB, 1.0, 2.0, 3.0, 4.0, and 5.0 mM of TMB was dried on a TMB pad, and a paper strip was constructed with individual pads. H_2O_2 was then applied to the TMB pad of the paper strips. According to the results, the intensity of the green-blue colour and the RGB ratio decreased with increasing TMB concentration (Fig. 6 a and b). This is because high concentration of TMB inhibits its function as a substrate [38]. Thus, the concentration of 1.0 mM was selected as the optimum amount of TMB.

Analysis of paper strips

After carrying out all optimizations, paper strips were assembled, and serial dilutions of H_2O_2 were applied onto the strips. The results shows that by increasing the concentration of H_2O_2, the intensity of the green-blue colour increased (Fig. 7 a). The respective RGB ratio graph indicates that the RGB ratio enhanced from 0.35 to 0.4 as the H_2O_2 concentration increased (Fig. 7 b). The highest RGB ratio was obtained for 5.0 mM of H_2O_2 and the lowest for 1.0 µM of H_2O_2, with a detection limit of 50.0 µM.

Interference assay

The interference of common semen components on detecting H_2O_2 was investigated (Fig. 8 a and b). The RGB ratio of the fructose group was similar to that of the H_2O_2 control group. In the citric acid group, a green-blue colour was produced, and its RGB ratio was less than the RGB ratio of the control and fructose groups (Fig. 8 b). In the ascorbic acid group, a pale green-blue

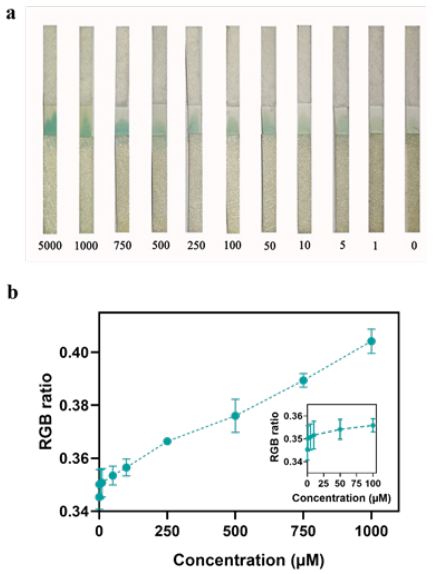

Fig. 7. The photograph of paper strip analysis with the various concentrations of H_2O_2 (a) and the RGB ratio curve quantifying the results of the paper strip analysis (b)

colour appeared, and its RGB ratio was the least compared to that of the other groups (Fig. 8 b).

As a result, fructose did not interfere with the H_2O_2 detection, while citric acid exhibited low interference, and ascorbic acid strongly interfered with H_2O_2 detection. The reason for the interference of citric acid and ascorbic acid

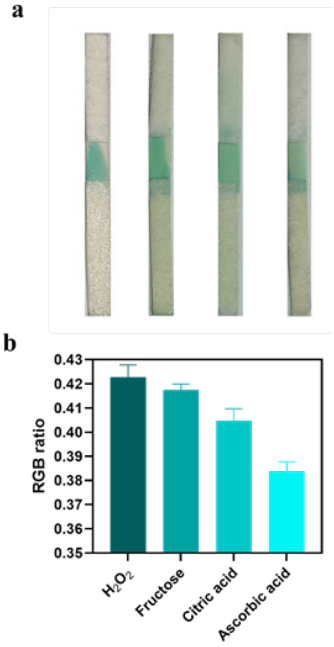

Fig. 8. The interference assay of the control group, fructose, citric acid, and ascorbic acid with H_2O_2 detection, the RGB ratio graphs (b)

on detecting H_2O_2 is that these two substances neutralize H_2O_2 as antioxidants, and by reducing the concentration of H_2O_2, the oxidation of TMB and the production of green-blue colour decreases. In addition, ascorbic acid can reduce blue-oxidized TMB to colourless TMB, and therefore, interferes with the performance of the paper strip [39, 40]. Although the concentration of ascorbic acid was less than that of citric acid, the ratio of their RGBs revealed that ascorbic acid interfered more with detecting H_2O_2 because ascorbic acid neutralizes H_2O_2 and reduces oxidized TMB [39].

Performance of LFA on real sample

The applicability of the paper strips was evaluated by monitoring H_2O_2 levels in human seminal plasma. After spiking H_2O_2 into seminal plasma samples, the samples were applied onto the TMB pad of the paper strips. The pale green-blue colour appeared for 750.0 µM and 1000.0 µM concentrations of H_2O_2. For lower concentrations, no significant green-blue colour was observed (Fig. 9). As seen in the interference section, some semen components, such as ascorbic acid, citric acid, uric acid and zinc prevented the oxidation of TMB by neutralizing H_2O_2, and ascorbic acid with its reducing properties, reduced the oxidized TMB and faded the blue color.

Thus, the detection limit of the paper strips in human seminal plasma was higher than that of the acetate buffer.

By comparing the results of paper strips with those of UV-visible spectroscopy, it is clear that the detection limit of UV-visible spectroscopy is lower than that of paper strips, similar to the results of other studies. For example, in a study conducted by Jia et al., H_2O_2 was detected using Fe_3O_4@chitosan nanoparticles, and the detection limit of UV-visible spectroscopy was 69 nM. In contrast, the detection limit of µPAD was 6.5 µM [41]. In another study by Tesfaye et al., the µPAD detection limit for nitrite and nitrate ions was 0.16 and 0.87 ppm, respectively. However, the detection limit of UV-visible spectroscopy was 0.066 and 0.1 ppm [42]. Looking at these reports and the results of our research, the sensitivity of paper-based diagnostic devices is less than that of the UV-visible spectroscopy method, which can be due to several reasons, such as the volume of nanoparticles and reagents used in UV-visible spectroscopy being more than that of paper-based devices. In addition, the heterogeneous distribution of nanoparticles and chromogens in the paper and the background noise created by the paper can be mentioned as reasons for the lower sensitivity of paper-based diagnostic methods [41]. On the other hand, the sensitivity in the paper strip and UV-visible methods decreased in the real sample compared to the buffer sample. However, as reported by Kullisaar et al., the concentration of H_2O_2 in infertile men with inflammation in the genital tract and oligospermic men without inflammation in the genital tract was in the range of 629-859 µM [27]. Therefore, the colorimetric method used in this study is able to detect such concentrations of H_2O_2 in real samples.

To date, two studies have been conducted on the measurement of H_2O_2 in semen using nanoparticles, and in both studies, the detection is based on the electrochemical method [4]. In a study by Blanco et al., they reported that fructose interfered with the detection of H_2O_2 and increased the signal by 20%. In another study by Promsuwan et al., the interference of components, such as ascorbic acid, in the detection of H_2O_2 were investigated, and they reported that none of them had any significant interference. However, in the present study, fructose did not cause any signal increase in the detection of H_2O_2, and ascorbic acid had the most significant interfering effect.

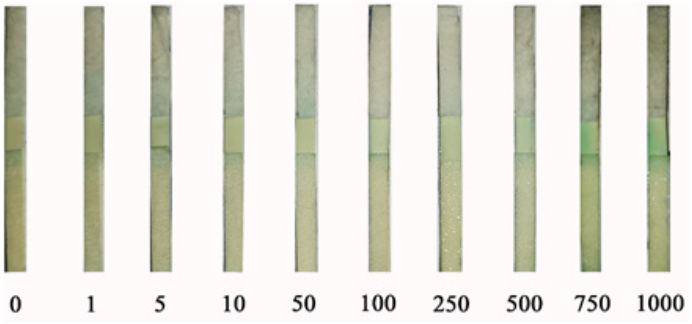

Fig. 9. The photograph evaluating the application of paper strips to detect H_2O_2 spiked into human seminal plasma

The main reason for the difference between the results of the current study and the previous studies is that the basis of the colorimetric assay is different from that of the electrochemical method, and in each of the methods, particular substrates, reagents, and materials are used.

Since the reported method is based on colorimetric analysis of the paper strips based on pictures captured on cell phones, with the help of a suitable mobile application, the quantification of the results can be realized with only access to a cell phone.

CONCLUSION

γ-Fe_2O_3@PB NPs were successfully fabricated and characterized. The results confirmed the formation of PB NPs coated γ-Fe_2O_3 NPs. A non-enzymatic paper strip based on the peroxidase-like activity of the γ-Fe_2O_3@PB NPs was designed and constructed. The paper strips performed well at a 1:25 dilution ratio of γ-Fe_2O_3@PB NPs and 1.0 mM of TMB. The interference assay revealed that citric acid and ascorbic acid interfered with the H_2O_2 detection. This interference is attributed to the ability of these antioxidants to neutralize H_2O_2 and reduce oxidized TMB to TMB, thus affecting colour production. The detection limits of paper strip for detecting H_2O_2 in acetate buffer and human semen samples were different because of the presence of antioxidant components in human semen specimens. It can be concluded that nanozymes exhibit a sensitive performance in detecting H_2O_2. However, their appropriate performance in biological environment is challenging because of a series of antioxidant components in some physiological fluids, which can interfere with the performance of nanozyme-based biosensors.

ACKNOWLEDGMENTS

This study was supported by Tehran University of Medical Sciences & Health Services, under grant number 1401-3-148-59267. The authors acknowledge Dr. Fatemeh Hataminia's help in the synthesis of nanoparticles.

CONFLICTS OF INTEREST

The authors report no conflict of interest.

REFERENCES

1. Yu Y, Pan M, Peng J, Hu D, Hao Y, Qian Z. A review on recent advances in hydrogen peroxide electrochemical sensors for applications in cell detection. Chin Chem Lett. 2022; 33(9): 4133-4135.
2. Manickam P, Vashist A, Madhu S, Sadasivam M, Sakthivel A, Kaushik A, et al., Gold nanocubes embedded biocompatible hybrid hydrogels for electrochemical detection of H_2O_2. Bioelectrochemistry. 2020; 131: 107373.
3. Peng L, Guo H, Wu N, Wang M, Hui Y, Ren H, et al. Fluorescent sensor based on bismuth metal-organic frameworks (Bi-MOFs) mimic enzyme for H_2O_2 detection in real samples and distinction of phenylenediamine isomers. Talanta. 2024; 272: 125753.
4. Blanco E, Vázquez L, Pozo M, Roy R, Petit-Domínguez M D, Quintana C, et al. Evaluation of oxidative stress: nanoparticle-based electrochemical sensors for hydrogen peroxide determination in human semen samples. Bioelectrochemistry. 2020; 135: 107581.
5. Ransy C, Vaz C, Lombès A, Bouillaud F. Use of H_2O_2 to cause oxidative stress, the catalase issue. Int J Mol Sci. 2020; 21(23): 9149.
6. Wang Z, Hong Y, Li J, Liu J, Jiang H, Sun L. Upconversion luminescent sensor for endogenous H_2O_2 detection in cells based on the inner filter effect of coated silver layer. Sens Actuators B Chem. 2023; 376: 132936.
7. Alsulami T, Alzahrani A. Enhanced nanozymatic activity on rough surfaces for H2O2 and tetracycline detection. Biosensors. 2024; 14(2): 106.
8. Gökçal B, Kip C, Şahinbaş D, Çelik E, Tuncel A, Silica microspheres functionalized with the iminodiacetic acid/copper (II) complex as a peroxidase mimic for use in metal affinity chromatography-based colorimetric determination of histidine-tagged proteins. Microchim Acta. 2020; 187: 1-9.
9. Shafa M, Ahmad I, Hussain S, Asif M, Pan Y, Zairov R, et al., Ag-Cu nanoalloys: An electrochemical sensor for H_2O_2 detection. Surf Interfaces. 2023; 36: 102616.
10. Li B, Wang R, Li G, Shen Q, Zou L, NiCoMnS/rGO nanocomposite for enzyme-free and ultrasensitive electrochemical catalysis of hydrogen peroxide and glucose. Microchem J. 2024; 199: 109947.
11. Zhang W, Lan Y, Chai D-F, Lv J, Dong G, Guo D, A novel "On-Off" colorimetric sensor for ascorbic acid and hydrogen peroxide based on peroxidase activity of CeO_2/Co_3O_4 hollow nanocubes. J Mol Struct. 2024; 1302: 137507.
12. Abedalwafa MA, Li Y, Ni C, Yang G, Wang L, Non-enzymatic colorimetric sensor strip based on melamine-functionalized gold nanoparticles assembled on polyamide nanofiber membranes for the detection of metronidazole. Anal Methods. 2019; 11(29): 3706-3713.
13. Ghasemi F, Fahimi-Kashani N, Bigdeli A, Alshatteri A H, Abbasi-Moayed S, Al-Jaf S H, et al., Paper based optical nanosensors–A review. Anal Chim Acta. 2023; 1238: 340640.
14. Hu J, Wang S, Wang L, Li F, Pingguan-Murphy B, Lu T J, et al., Advances in paper-based point-of-care diagnostics. Biosens Bioelectron. 2014; 54: 585-597.
15. Dkhar D S, Kumari R, Malode S J, Shetti N P, Chandra P, Integrated lab-on-a-chip devices: Fabrication methodologies, transduction system for sensing purposes. J Pharm Biomed Anal. 2023; 223: 115120.
16. Atabakhsh S, Abbasali HH, and Ashtiani SJ, Thermally programmable time delay switches for multi-step assays in paper-based microfluidics. Talanta. 2024; 271: 125695.
17. Shirshahi V and Afrapoli ZB, Lateral flow assay with green nanomaterials. Comprehensive Analytical Chemistry. 2023; 105: 301-330.
18. Fung, KK, Chan CPY, Renneberg R. Development of enzyme-based bar code-style lateral-flow assay for hydrogen peroxide determination. Anal Chim Acta. 2009; 634(1): 89-

95.
19. Chi Z, Wang Q, and Gu J, Recent advances of colorimetric sensors based on nanozymes with peroxidase-like activity. Analyst. 2022; 148(3): 487-506.
20. Tan W, Yao G, Yu H, He Y, Lu M, Zou T, et al., Ultra-trace Ag doped carbon quantum dots with peroxidase-like activity for the colorimetric detection of glucose. Food Chem. 2024; 447: 139020.
21. Niu X, Cheng N, Ruan X, Du D, Lin Y, Nanozyme-based immunosensors and immunoassays: recent developments and future trends. J Electrochem Soc. 2020; 167(3): 037508.
22. Jabiyeva N, Çakıroğlu B, and Özdemir A, The peroxidase-like activity of Au NPs deposited inverse opal CeO_2 nanozyme for rapid and sensitive H_2O_2 sensing. J Photochem Photobiol A Chem. 2024; 452: 115576.
23. Song C, Ding W, Zhao W, Liu H, Wang J, Yao Y, et al., High peroxidase-like activity realized by facile synthesis of FeS_2 nanoparticles for sensitive colorimetric detection of H_2O_2 and glutathione. Biosens Bioelectron. 2020; 151: 111983.
24. Çakıroğlu B, Graphene quantum dots on TiO2 nanotubes as a light-assisted peroxidase nanozyme. Microchim Acta. 2024; 191(5): 1-10.
25. Marvi P K, Ahmed S R, Das P, Ghosh R, Srinivasan S, Rajabzadeh A R, Prunella vulgaris-phytosynthesized platinum nanoparticles: Insights into nanozymatic activity for H_2O_2 and glutamate detection and antioxidant capacity. Talanta. 2024; 274: 125998.
26. Dutta S, Majzoub A, and Agarwal A, Oxidative stress and sperm function: A systematic review on evaluation and management. Arab J Urol. 2019; 17(2): 87-97.
27. Kullisaar T, Türk S, Kilk K, Ausmees K, Punab M, Mändar R, Increased levels of hydrogen peroxide and nitric oxide in male partners of infertile couples. Andrology. 2013; 1(6): 850-858.
28. Promsuwan K, Soleh A, Saisahas K, Saichanapan J, Thiangchanya A, Phonchai A, et al., Micro-colloidal catalyst of palladium nanoparticles on polyaniline-coated carbon microspheres for a non-enzymatic hydrogen peroxide sensor. Microchem J. 2021; 171: 106785.
29. Sun Y-k, Ma M, Zhang Y, Gu N, Synthesis of nanometer-size maghemite particles from magnetite. Colloids Surf A Physicochem Eng Asp. 2004; 245(1-3): 15-19.
30. Zhang X-Q, Gong S-W, Zhang Y, Yang T, Wang C-Y, Gu N, Prussian blue modified iron oxide magnetic nanoparticles and their high peroxidase-like activity. J Mater Chem. 2010; 20(24): 5110-5116.
31. Zhang W, Niu X, Li X, He Y, Song H, Peng Y, et al., A smartphone-integrated ready-to-use paper-based sensor with mesoporous carbon-dispersed Pd nanoparticles as a highly active peroxidase mimic for H_2O_2 detection. Sens Actuators B Chem. 2018; 265: 412-420.
32. Sikirzhytskaya A, Sikirzhytski V, Pérez-Almodóvar L, Lednev I K, Raman spectroscopy for the identification of body fluid traces: semen and vaginal fluid mixture. Forensic Chem. 2023; 32: 100468.
33. Videla E, Blanco A M, Galli M E, FERNÁNDEZ-COLLAZO E, Human seminal biochemistry: fructose, ascorbic acid, citric acid, acid phosphatase and their relationship with sperm count. Andrologia. 1981; 13(3): 212-214.
34. Pyrasch M and Tieke B, Electro-and photoresponsive films of Prussian blue prepared upon multiple sequential adsorption. Langmuir. 2001; 17(24): 7706-7709.
35. Estelrich J and Busquets M A, Prussian blue: a nanozyme with versatile catalytic properties. Int J Mol Sci. 2021; 22(11): 5993.
36. Dutta A K, Maji S K, Srivastava D N, Mondal A, Biwas P, Paul P, et al., Peroxidase-like activity and amperometric sensing of hydrogen peroxide by Fe2O3 and Prussian Blue-modified Fe2O3 nanoparticles. J Mol Catal A Chem. 2012; 360: 71-77.
37. Misro M M, Choudhury L, Upreti K, Gautam D, Chaki S P, Mahajan A S, et al., Use of hydrogen peroxide to assess the sperm susceptibility to oxidative stress in subjects presenting a normal semen profile. Int J Androl. 2004; 27(2): 82-87.
38. Aslanzadeh S, Ishola M M, Richards T, Taherzadeh M J, An overview of existing individual unit operations. Biorefineries, 2014; 3-36.
39. Shu X, Chang Y, Wen H, Yao X, Wang Y, Colorimetric determination of ascorbic acid based on carbon quantum dots as peroxidase mimetic enzyme. RSC Adv. 2020; 10(25): 14953-14957.
40. Fan X, Bao Y, Chen Y, Wang X, On S L W, Wang J, Synthesis of β-Cyclodextrin@ gold nanoparticles and its application on colorimetric assays for ascorbic acid and Salmonella based on peroxidase-like activities. Biosensors. 2024; 14(4): 169.
41. Jia S, Zhang X, Yuan F, Xia T, Colorimetric test paper for H_2O_2 determination based on peroxidase-like activity of an AuFe/ZIF-8-graphene composite. ChemistrySelect. 2022; 7(43): e202202984.
42. Tesfaye T and Hussen A, Microfluidic paper-based analytical device (μPAD) fabricated by wax screen printing technique for the determination of nitrite and nitrate ion in water samples. Microfluid Nanofluidics. 2022; 26(3): 22.